Journal of Nuclear Materials 406 (2010) 345–350

Contents lists available at ScienceDirect

Journal of Nuclear Materials

journal homepage: www.elsevier.com/locate/jnucmat

Ab initio simulation of yttrium oxide nanocluster formation on *fcc* Fe lattice

Aleksejs Gopejenko [a,*], Yuri F. Zhukovskii [a], Pavel V. Vladimirov [b], Eugene A. Kotomin [a], Anton Möslang [b]

[a] *Institute of Solid State Physics, University of Latvia, Kengaraga Str. 8, LV-1063 Riga, Latvia*
[b] *Karlsruhe Institute of Technology, Institute for Materials Research-I, P.O. Box 3640, 76021 Karlsruhe, Germany*

ARTICLE INFO

Article history:
Received 15 March 2010
Accepted 7 September 2010

ABSTRACT

Using results of density functional theory (DFT) calculations the first attempt towards the understanding of Y_2O_3 particles formation in oxide dispersed strengthened (ODS) ferritic–martensitic steels was performed. The present work includes modeling of single defects (O impurity atom, Fe vacancy and Y substitute atom), interaction between substituted Y atoms, Y–Fe vacancy pairs and oxygen impurity atoms in the iron matrix. The calculations have showed the repulsive interaction between the two Y substitute atoms at any separation distances that might mean that the oxygen atoms or O atoms with vacancies are required to form binding between atoms in the yttrium oxide nanoclusters.

1. Introduction

Oxide dispersion strengthened (ODS) structures of reduced activation ferritic–martensitic (RAFM) steels are considered as promising construction materials for fusion reactor applications [1]. Application of the ODS steels strengthened by Y_2O_3 precipitates instead of their non-strengthened counterparts permits to increase the operating temperatures of blanket structures by 100 °C [2,3]. Both size and spatial distribution of oxide particles significantly affect mechanical properties and radiation resistance of ODS steels which are produced by mechanical alloying for several tens of hours, followed by a hot isostatic pressing (hipping) at temperature around 1000–1200 °C and pressure ~100 MPa. The mechanism of ODS particle formation is not completely understood yet. There is experimental evidence that after milling a noticeable part of Y and O atoms can be decomposed from yttria clusters in steel matrix with concentrations above their equilibrium solubility [4,5]. If this is indeed the case, precipitation of Y_2O_3 nanoparticles can occur already at the hipping stage as a result of yttrium–oxygen co-precipitation.

The two-step theoretical approach for atomistic simulation of this process is proposed. The *first step* includes extensive *ab initio* calculations of elementary yttrium and oxygen complexes inside the iron lattice containing also Fe vacancies. Both interaction energies between solute and matrix atoms and barriers for diffusion of different solute atoms are extracted from these calculations for further atomistic simulations.

The *second step* (not performed in this paper) consists in the study of precipitate growth based on results of *ab initio* calculations and employs the lattice kinetic Monte Carlo (LKMC) simulations on the matrix and interstitial sublattices. Matrix sublattice is used for iron atoms and substitutional solutes (yttrium), while oxygen resides inside the octahedral and tetrahedral interstitial lattice sites. Direct exchange of metal atoms was considered in recent simulations on ODS steels, in order to minimize the system free energy [5–7]. In reality, the diffusion of precipitating components occurs inside the matrix lattice and therefore small precipitates are coherent with it. As precipitate grows its bulk energy becomes more substantial than the energy of matrix–precipitate interface and therefore the precipitates might undergo phase transition to the more stable phase loosing their original coherence with the matrix.

Iron is a basic element for steel making that explains enhanced interest during the last years to iron atomistic simulations (for both α- and γ-Fe phases) and its alloys, particularly based on periodic first-principles DFT calculations [8–14]. Transition between the α- and γ-phases in steels depends, in particular, on the chromium content in the matrix, vanishing completely above 14% Cr. While 9% Cr ferritic–martensitic steels undergo transition to the face-centered-cubic (*fcc*) γ-phase at hipping temperatures, 14% Cr ferritic steels are staying completely in the body-centered-cubic (*bcc*) α-phase. Unlike the *ferromagnetic* α-Fe, the *fcc* γ-Fe phase, which is known experimentally to be paramagnetic, is predicted by *ab initio* simulations, which are effectively performed at 0 K, to be *paramagnetic*, *antiferromagnetic*, *ferromagnetic*, or *revealing a spin-density wave*, *i.e.*, magnetically unstable, depending on the lattice constant and structural distortion [8]. The γ-Fe phase is thermodynamically stable in the temperature range between 1173 and 1660 K only; at lower temperatures it was observed in the form of either small iron precipitates inside the *fcc* copper matrix or ultrathin Fe layers grown on the densely-packed Cu substrates

* Corresponding author.
E-mail address: gopeenko@latnet.lv (A. Gopejenko).

0022-3115/$ - see front matter © 2010 Elsevier B.V. All rights reserved.
doi:10.1016/j.jnucmat.2010.09.005

[10]. The *cubic symmetry* of γ-Fe lattice is broken along the transition from paramagnetic to antiferromagnetic ordering, being unstable against small tetragonal and orthorhombic distortions, whereas monoclinic shearing of cubic lattice usually stabilizes the ferromagnetic state [9]. The *fcc* ↔ *bcc* phase transitions were observed in very thin films with (0 0 1) surfaces as well as bulk crystal of γ-Fe and α-Fe subjected to biaxial strains [11,12] which were found to be correlated with softening of the strain-induced elastic moduli.

The DFT calculations on the Y–Ti–O nanoclusters within *bcc* Fe matrix were performed recently [15,16]. The results of both studies contradict to each other. The main conclusion made in Ref. [15] is that the presence of preexisting vacancies significantly decreases the formation energy of O-vacancy pairs which leads to the increase of oxygen atoms concentration. This enables the nucleation of O enriched nanoclusters that attract Y and Ti atoms. However, the calculations performed in Ref. [16] showed that Y–Ti–O nanocluster formation may occur without the energetic assistance of the preexisting vacancies.

This paper is aimed to describe the formation of Y_2O_3 nanoclusters on γ-Fe lattice that corresponds to low-Cr steels hipped above the α–γ transition temperature. Of course, the choice of the reference state is complicated due to the fact that paramagnetic γ-Fe is not stable at zero temperatures, however, as the formation of Y_2O_3 nanoclusters occurs at the temperatures of ∼1373 K, where γ-Fe is paramagnetic, the model based on the non-magnetic *fcc* iron lattice is used in the calculations. These calculations have been performed by us using maximum amount of computational resources available to us. Taking into account these limitations, it would be rather problematic to improve the model by including spin-polarization in the calculations with the aim to perform averaging over various spin orientations. Moreover, such approach would probably give only a small correction to the non-magnetic calculations implemented in this work.

The following results of *ab initio* calculations are present in this paper: (i) perfect and defective iron lattice with varying content of Fe vacancies, (ii) O impurity atom (estimating also the energy barrier for its migration in γ-Fe lattice), (iii) one or two Y substitute atoms at different interatomic distances, and (iv) various pair configurations of Y substitute atom and Fe vacancy. Their implications to the oxide nanocluster formation are discussed.

2. Computational details

VASP-4.6 computer code with a plane-wave basis set [17,18] has been used for large-scale first-principles calculations on both perfect and defective *fcc* lattice of γ-Fe phase. Perdew–Wang-91 GGA (Generalized Gradient Approximation) non-local exchange–correlation functional [19] and the scalar relativistic PAW (Projector-Augmented Wave) pseudopotentials [20] have been used for these parallel calculations with a full geometry optimization. The pseudopotentials describe the core electrons of Fe ($4s^1 3d^7$ outer shell), O ($2s^2 2p^4$) and Y ($4s^2 4p^6 5s^1 4d^2$) atoms with 8, 6 and 11 external electrons, respectively. Magnetic effects have not been taken into account since a cubic γ-Fe is known to be paramagnetic in the temperature range of its stability as mentioned above.

A series of preliminary calculations has been performed to define the parameters of the calculations reproducing the experimental data (for example, lattice constant, bulk modulus and cohesive energy *per* atom in γ-Fe). This includes an analysis how the convergence of the results depends on the supercell size, the cut-off energy and the *k*-point set in the corresponding Brillouin zone. We have found that the calculations of the commonly used 27-atom $3 \times 3 \times 3$ supercell are still inaccurate, due to a small size of the supercell which causes the noticeable elastic interactions between defect and its periodical image. Thus, the supercell has been extended to 64 atoms with the $4 \times 4 \times 4$ enlarged translation vectors of the unit cell. For the calculations on the yttrium atom pair in the iron lattice, even larger, at least $4 \times 4 \times 6$ (96-atom) supercell is required, which symmetry is lower.

The cut-off energy has been varied from 300 to 1200 eV and the *k*-point set from 64 ($4 \times 4 \times 4$) to 4096 ($16 \times 16 \times 16$). It has been found that the results are reliably converged only beginning with the unusually large cut-off energy of 800 eV (*cf.* the default cut-off energy of 267 eV), while varying the *k*-point mesh it has been found that at least $12 \times 12 \times 12$ mesh allows us to obtain more-or-less plausible results.

In this paper, we present the optimized structures of γ-Fe supercells containing: (i) single defects, *i.e.*, Fe vacancies and impurity atoms (Figs. 1–3), (ii) pairs of point defects (Figs. 4 and 5) and (iii) triple point defects (Fig. 6) as well as the corresponding plots of the electron density re-distributions caused by these defects (Figs. 1–6). For each defect, we have estimated also the electronic charge transfer and formation energy (Section 3).

3. Main results

Firstly, we have verified our computational procedure for key properties of perfect γ-Fe single crystal as determined earlier both experimentally and theoretically [8–14]. The equilibrium lattice constant, bulk modulus and cohesive energy for a cubic paramagnetic γ-Fe lattice have been calculated to be (i) 3.44 Å, (ii) 162 GPa and (iii) 4.96 eV/atom, respectively. These values agree qualitatively with the results of other *ab initio* calculations on the same structure: (i) 3.40–3.60 Å [8,10,12], (ii) 171–211 GPa [8,11] and (iii) 4.42 eV/atom [11], respectively, as well as with experimental values of: (i) 3.57 Å [13], (ii) 133–164 GPa [14] for γ-Fe, which can exist in different magnetic states as mentioned above, and (iii) 4.28 eV/atom [10] for a low-temperature ferromagnetic α-Fe which is believed to be close to cohesive energy of γ-Fe.

The formation energy of single vacancy in a $4 \times 4 \times 4$ γ-Fe supercell, which is surrounded by 12 nearest iron atoms forming cuboctahedron, has been found to be 2.37 eV accompanied with 0.75% and ∼0.5% inward relaxation of the two nearest coordination shells, respectively (Fig. 1). Presence of single Fe vacancy noticeably re-distributes the electronic density as shown in Fig. 1.

Our calculations performed for the same γ-Fe supercell predict that the oxygen atoms reside on either octahedral *O* (six nearest Fe neighbors, Fig. 2) or tetrahedral *T* (four nearest Fe neighbors) interstitial positions. The latter has been found to be ∼0.1–0.2 eV less favorable than the former, in accordance with the results of theoretical simulations of oxygen absorbed in the *fcc* Al lattice [21]. The excessive electronic charge attracted by oxygen impurity in *O* center of γ-Fe lattice achieves ∼1.4*e* (*cf.* 1.8*e* for the same position of oxygen atom in *fcc* Al lattice [21]). The oxygen absorption results in a considerable expansion of the two nearest coordination shells around an impurity atom (∼9.0% and 1.75%, respectively, in octahedral interstitial). A barrier for oxygen atom migration between the nearest *O* and *T* positions has been found to be 1.1 eV (*cf.* 1.72–1.75 eV, according to various experimental studies systematized in the handbook [22]). Experimental value might be affected by O–Fe vacancy binding which is pronounced for α-Fe as shown recently [23].

The calculations of Y atom in γ-Fe lattice have been performed taking into account that the Y atom is placed on the regular site of Fe lattice. The Y substitute atom donates the electronic density to the nearest Fe neighbors (∼1*e per* atom). The formation energy of the Y-substitution defect in the γ-Fe lattice is estimated to be 0.48 eV for the $4 \times 4 \times 4$ supercell, with the 7% and ∼2% expansion of the two nearest coordination shells, respectively (Fig. 3). At the

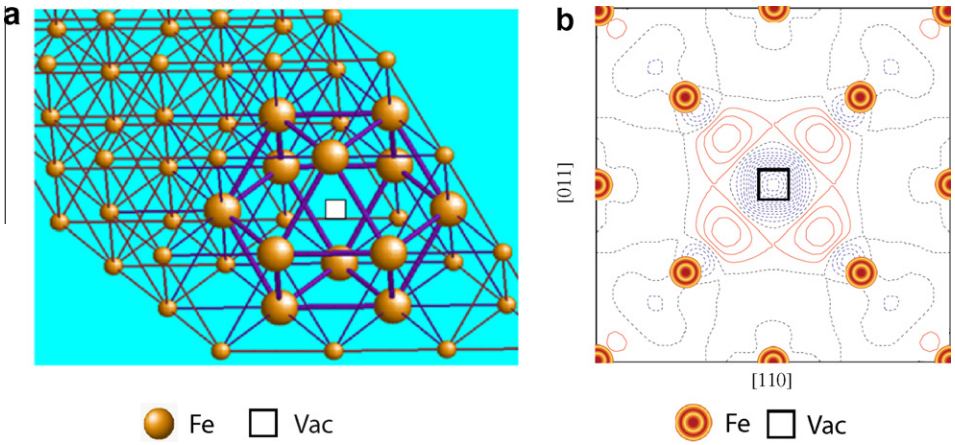

Fig. 1. The model of the vacancy in the γ-Fe crystalline lattice (a) and the corresponding charge re-distribution around the Fe vacancy inside the (1 1 0) plane (b). The latter is defined as the total electron density in the perfect bulk γ-Fe lattice minus the sum of the electronic densities of defective γ-Fe lattice and single iron atom in vacuum (which coordinates coincide with those of a vacancy). Dash-dotted (black) isolines correspond to the zero level, dashed (blue) lines stand for a decrease of the electron density whereas solid (red) for a density increase. Density increment between isolines is 0.002e Å^{-3}. (For interpretation of the references to colour in this figure legend, the reader is referred to the web version of this article.)

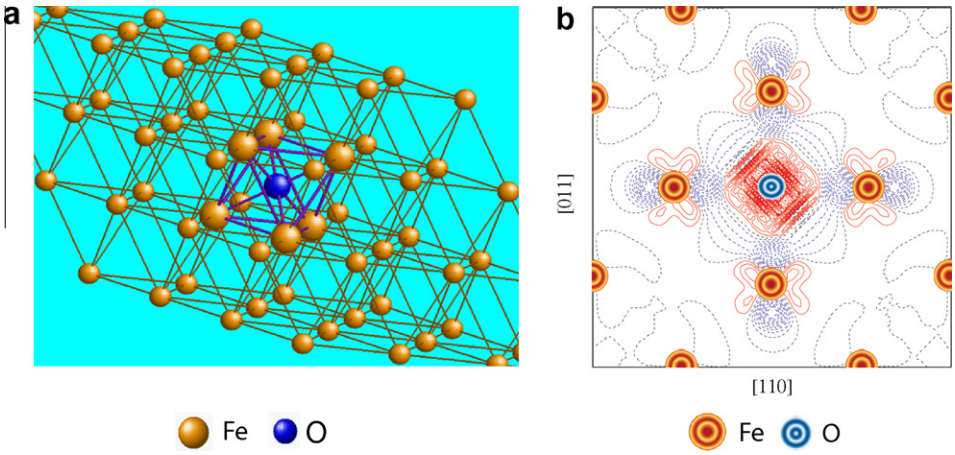

Fig. 2. The model of the γ-Fe crystalline lattice with the oxygen impurity atom (a) and the corresponding charge re-distribution around the O atom inside the (1 1 0) plane (b). The latter is defined as the total electron density γ-Fe lattice with O impurity atom minus the sum of those for iron lattice (with relaxation as in the case of O doping) and oxygen atom in vacuum. For details, see explanations given in the caption to Fig. 1.

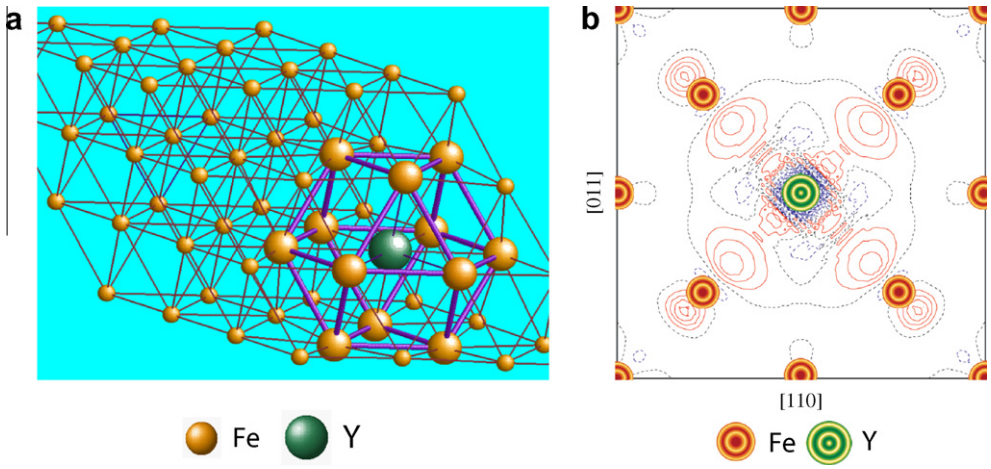

Fig. 3. The model of the γ-Fe crystalline lattice with a single Y substitute atom (a) and the corresponding charge re-distribution around the Y substitute inside the (1 1 0) plane (b). The latter is defined as the total electron density of γ-Fe lattice with Y substitute atom minus the sum of those for γ-Fe lattice with vacancy and yttrium atom in vacuum. For details, see explanations given in the caption to Fig. 1.

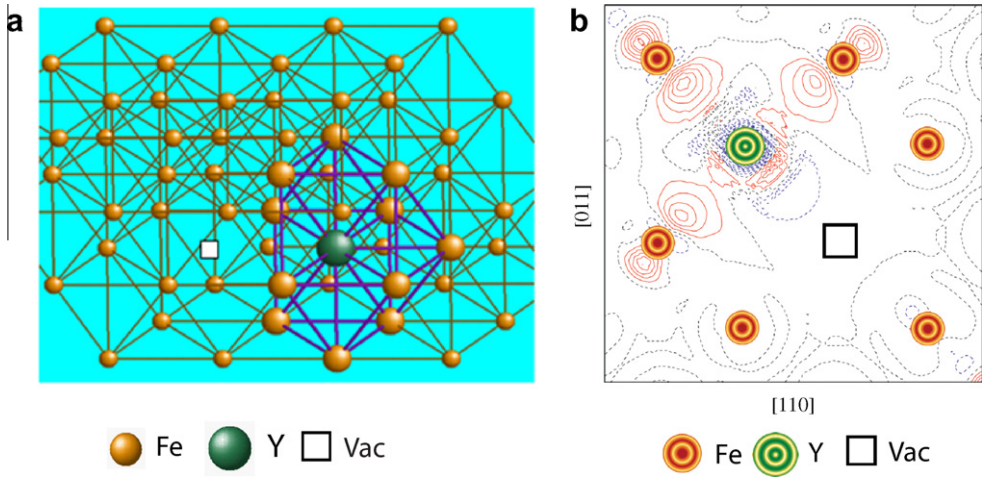

Fig. 4. The model of the γ-Fe crystalline lattice, containing Y substitute atom and Fe vacancy in the 1st nearest neighbors positions (a) and the corresponding charge re-distribution around the Y substitute and Fe vacancy inside the (1 1 0) plane (b). The latter is defined as the total electron density of γ-Fe lattice with one Y substitute atom minus the sum of those for γ-Fe lattice with two vacancies and yttrium atom in vacuum. For details, see explanations given the caption to in Fig. 1.

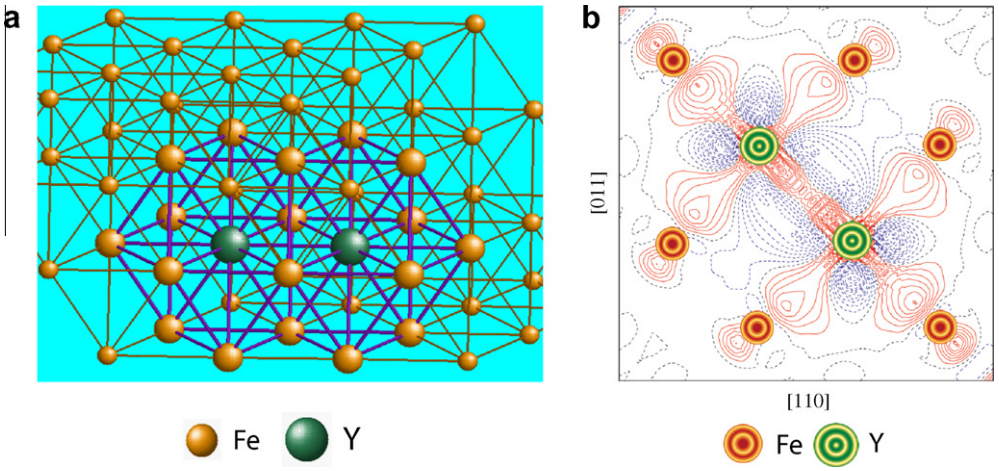

Fig. 5. The model of the γ-Fe crystalline lattice with 2Y substitute atoms in the 1st nearest neighbors positions (a) and the corresponding charge re-distribution around the 2Y substitutes inside the (1 1 0) plane (b). The latter is defined as the total electron density of γ-Fe lattice with 2Y substitute atoms minus the sum of those for defective γ-Fe lattice and two yttrium atoms in vacuum. For details, see explanations given in the caption to Fig. 1.

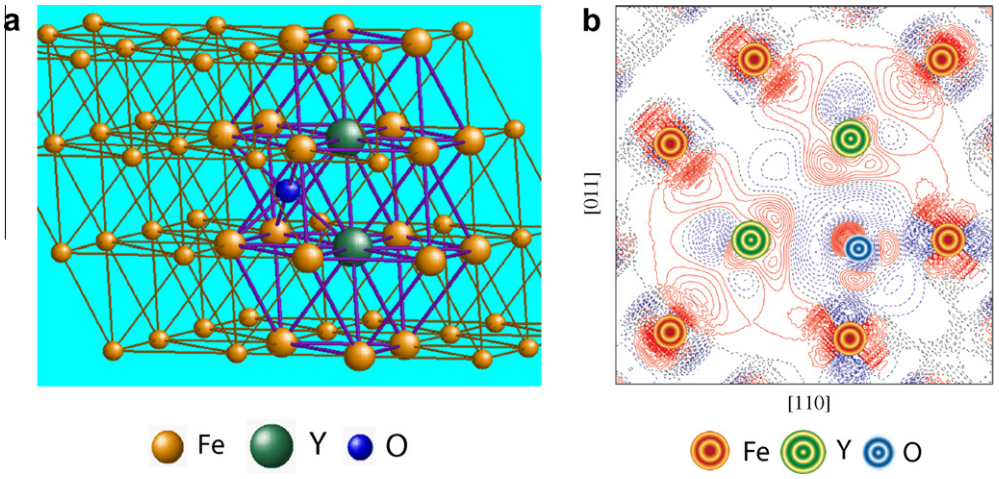

Fig. 6. The model of the γ-Fe crystalline lattice with 2Y substitutes and 1 O impurity atom in the 1st nearest neighbors positions (a) and the corresponding charge re-distribution around the 2Y substitutes and O atom inside the (1 1 0) plane (b). The latter is defined as the total electron density of γ-Fe lattice including the two Y substitutes and O impurity atom minus the sum of those for γ-Fe lattice with two vacancies, as well as 2Y and O atoms in vacuum. For details, see explanations given in the caption to Fig. 1.

Table 1
The binding[a] and formation[b,c] energies of the Y substitute and Fe vacancy calculated in the γ-Fe lattice for the 4 × 4 × 4 supercell.

Configuration	4 × 4 × 4 supercell	
	E_f (eV)	E_b (eV)
Y–Fe vacancy-1-NN	1.19	1.67
Y–Fe vacancy-2-NN	3.07	−0.21
Y–Fe vacancy-3-NN	2.57	0.30
Y–Fe vacancy-4-NN	2.47	0.40

$$^{a}E_{b\,Y-Vac} = E_{f\,Y} + E_{f\,Vac} - E_{f\,Y-Vac}, \quad (1a)$$

$$^{b}E_{f\,Y} = E_{conf\,Y} - \frac{N-1}{N}E_{conf\,id} - E_{coh\,Y}, \quad (1b)$$

$$^{c}E_{f\,Y-Vac} = E_{conf\,Y-Vac} - \frac{N-2}{N}E_{conf\,id} - E_{coh\,Y}, \quad (1c)$$

where N is the number of atoms in the supercell, $E_{conf\,id}$ the total energy of the calculated ideal configuration, $E_{coh\,Y}$ the cohesive energy of Y, $E_{f\,Y}$ and $E_{f\,Y-Vac}$ the formation energies of one Y atom and Y–Fe vacancy pair in the Fe lattice, respectively, $E_{conf\,Y}$ and $E_{conf\,Y-Vac}$ the total energies of the calculated supercell with one Y substitute and Y–Fe vacancy pair, respectively, E_{bY-Vac} the binding energy of the Y–Fe vacancy pair in the γ-Fe lattice, and $E_{f\,Vac}$ the formation energy of Fe vacancy:

$$E_{f\,Vac} = E_{conf\,Vac} - \frac{N-1}{N}E_{conf\,id}$$

Table 2
The binding and formation energies of the two Y atom substitutes calculated in the γ-Fe lattice for the 4 × 4 × 4 supercell.

Configuration	4 × 4 × 4 supercell	
	E_f (eV)[a]	E_b (eV)[a]
Y–Y-1-NN	1.72	−0.73
Y–Y-2-NN	1.43	−0.45
Y–Y-3-NN	1.44	−0.46
Y–Y-4-NN	2.03	−1.05

[a] Definitions of E_f and E_b values are similar to those described in footnotes for Table 1.

same time, the Y atom inserted in the *fcc* Fe lattice is rather affected by repulsion from the nearest Fe neighbors as follows from the electron charge re-distribution.

At the next step, we have simulated configurations of defect pairs. The calculations on the interaction between the Y substitutional atom and Fe vacancy at different inter-distances have been performed first (Fig. 4). The results of these calculations are presented in Table 1 (formation and binding energies of the pair of yttrium atoms are defined in the footnotes) which clearly shows that the attraction is found for the 1-NN, 3-NN and 4-NN configurations while the repulsion is observed for the 2-NN configuration (Table 1). The relative displacement of Y atom towards Fe vacancy in the 1-NN configurations is the most significant (1.25 Å) as far as Y occupies intermediate position between two vacant lattice sites and the binding energy for this configuration is the largest (1.67 eV). The repulsive interaction between Y atom and Fe vacancy at 2-NN site might be caused by the two iron atoms which are positioned at 1-NN sites relatively to both point defects leading to the displacement of this Y atom away from the both neighboring iron atoms and Fe vacancy.

The interaction between two Y substitutional atoms at different separation distances (1-NN, 2-NN, 3-NN and 4-NN) has been calculated too (Fig. 5). No binding has been found between the two yttrium atoms in the iron lattice at any distance (Table 2). Since we have observed a light repulsion between the single Y substitute atom and surrounding Fe atoms (Fig. 3) some enhancement of electron density between Y–Y pair can be visible as compared to the configuration of yttrium atom and iron vacancy (Fig. 4), *i.e.*, the repulsion between the two Y substitute atoms is smaller than that between Y and Fe atoms.

To construct the more stable configuration of solute atoms, we have added to the pair of Y substitute atoms (1-NN neighbors) an oxygen atom positioned at the *O* site and have calculated three-atom configuration (Fig. 6). No binding was found in this nanocluster inside the γ-Fe lattice as compared to Y–O–Y motif existing in bixbyite structure of Y_2O_3. Significant displacements were observed during relaxation between each pair of Y and O atoms, increasing Y–O distance by 0.45 Å, whereas Y atoms move from each other by 0.37 Å. Obviously, existing Y–O–Y configuration inside the γ-Fe lattice does not correspond to the Y–O–Y structure of the nearest oxygen and yttrium atoms in any Y_2O_3 crystalline phase [24]. Thus, a quite complicated field of the interactions is formed at the initial stage of Y_2O_3 precipitate growth inside iron crystalline matrix.

As the binding energy was not found between the atoms in such a Y–O–Y quasi-molecule, the configuration containing two Y atoms, O atom and Fe vacancy has been recently calculated and quite noticeable binding energy between the atoms in this nanocluster has been found. These results are planned to be analyzed in our next paper.

4. Conclusions

We have performed a series of large-scale first-principles calculations on perfect γ-Fe lattice as well as on that containing a single Fe atom vacancy, oxygen impurity atom, single Y substitute atom, pairs of Y with either Fe vacancy or Y atom, and three-atom cluster Y–O–Y. This allows us to determine accurately the pair- and triple-wise interaction energies necessary for further kinetic Monte Carlo simulations. Attraction between the Y substitute and Fe vacancy has been found for the 1-NN, 3-NN and 4-NN configurations whereas no binding has been observed between the two Y atoms in *fcc* Fe lattice. Not only the addition of O atom to the pair of Y atoms is required to obtain a certain binding between the impurity atoms but also the Fe vacancies should be included in the supercell model for creation of binding between the Y and O atoms in nanoclusters.

Acknowledgements

This work, supported in part by the European Social Fund Project No. 2009/0202/1DP/1.1.1.2.0/09/APIA/VIAA/141, by Euroatom Fission and Euroatom Mobility Programs, the European Communities under the contract of Association between EURATOM and Karlsruhe Institute of Technology as well as between EURATOM and University of Latvia (AEUL) has been carried out within the framework of the European Fusion Development Agreement. The views and opinions expressed herein do not necessarily reflect those of the European Commission. Technical assistance of D. Bocharov is highly appreciated.

References

[1] R. Lindau, A. Möslang, M. Rieth, M. Klimiankou, E. Materna-Morris, A. Alamo, A.-A.F. Tavassoli, C. Cayron, A.-M. Lancha, P. Fernández, N. Baluc, R. Schäublin, E. Diegele, G. Filacchioni, J.W. Rensman, B. Van der Schaaf, E. Lucon, W. Dietz, Fusion Eng. Des. 75–79 (2005) 989–996.
[2] M. Klimiankou, R. Lindau, A. Möslang, J. Nucl. Mater. 367–370 (2007) 173–178.
[3] R. Lindau, A. Möslang, M. Schirra, P. Schlossmacher, M. Klimiankou, J. Nucl. Mater. 307–311 (2002) 769–772.
[4] T. Okuda, M. Fujiwara, J. Mater. Sci. Lett. 14 (1995) 1600–1603.
[5] G.R. Odette, M.J. Alinger, B.D. Wirth, Ann. Rev. Mater. Res. 38 (2008) 471–503.
[6] M.J. Alinger, B.D. Wirth, H.-J. Lee, G.R. Odette, J. Nucl. Mater. 367–370 (2007) 153–159.
[7] C. Hin, B.D. Wirth, J.B. Neaton, Phys. Rev. B 80 (2009) 134118.
[8] H.C. Herper, E. Hoffmann, P. Entel, Phys. Rev. B 60 (1999) 3839–3848.
[9] D. Spišák, J. Hafner, Phys. Rev. Lett. 88 (2002) 056101.

[10] M. Marsman, J. Hafner, Phys. Rev. B 66 (2002) 224409.
[11] W. Zhong, G. Overney, D. Tománek, Phys. Rev. B 47 (1993) 95–99.
[12] J.T. Wang, D.S. Wang, Y. Kawazoe, Appl. Phys. Lett. 88 (2006) 132513.
[13] V.L. Moruzzi, P.M. Marcus, K. Schwarz, P. Mohn, Phys. Rev. B 34 (1986) 1784–1791.
[14] G. Ghosh, G.B. Olson, Acta Mater. 50 (2002) 2655–2675.
[15] C.L. Fu, M. Krčmar, G.S. Painter, X.-Q. Chen, Phys. Rev. Lett. 99 (2007) 225502.
[16] Y. Jiang, J.R. Smith, G.R. Odette, Phys. Rev. B 79 (2009) 064103.
[17] G. Kresse, J. Hafner, VASP the Guide, University of Vienna, 2007. <http://www.cms.mpi.univie.ac.at/vasp/>.
[18] G. Kresse, J. Furthmueller, Phys. Rev. B 54 (1996) 11169–11186.
[19] J.P. Perdew, Y. Wang, Phys. Rev. B 45 (1992) 13244–31249.
[20] G. Kresse, D. Joubert, Phys. Rev. B 59 (1999) 1758–1775.
[21] Yu.F. Zhukovskii, P.W.M. Jacobs, M. Causà, J. Phys. Chem. Solids 64 (2003) 1317–1331.
[22] H. Mehrer (Ed.), Diffusion in Solid Metals and Alloys, Landolt–Bernstein, New Series III, vol. 26, Springer, Berlin, 1990, p. 481.
[23] M.K. Miller, C.L. Fu, M. Krčmar, D.T. Hoelzer, C.T. Liu, Front. Mater. Sci. China 3 (1) (2009) 9–14.
[24] V. Swamy, H.J. Seifert, F. Aldinger, J. Alloys Compd. 269 (1998) 201–207.